mathematics

MDPI

Article

Heat and Mass Transfer Analysis for the Viscous Fluid Flow: Dual Approximate Solutions

Remus-Daniel Ene [1,†], Nicolina Pop [2,*,†] and Rodica Badarau [3,†]

[1] Department of Mathematics, Politehnica University of Timisoara, 2 Victoria Square, 300006 Timisoara, Romania
[2] Department of Physical Foundations of Engineering, Politehnica University of Timisoara, 2 Vasile Parvan Blvd, 300223 Timisoara, Romania
[3] Department of Mechanical Machines, Equipment and Transportation, Politehnica University of Timisoara, 1 Mihai Viteazul Blvd., 300222 Timisoara, Romania
* Correspondence: nicolina.pop@upt.ro
† These authors contributed equally to this work.

Abstract: The aim of this paper is to investigate effective and accurate dual analytic approximate solutions, while taking into account thermal effects. The heat and mass transfer problem in a viscous fluid flow are analytically explored by using the modified Optimal Homotopy Asymptotic Method (OHAM). By using similarity transformations, the motion equations are reduced to a set of nonlinear ordinary differential equations. Based on the numerical results, it was revealed that there are dual analytic approximate solutions within the mass transfer problem. The variation of the physical parameters (the Prandtl number and the temperature distribution parameter) over the temperature profile is analytically explored and graphically depicted for the first approximate and the corresponding dual solution, respectively. The advantage of the proposed method arises from using only one iteration for obtaining the dual analytical solutions. The presented results are effective, accurate and in good agreement with the corresponding numerical results with relevance for further engineering applications of heat and mass transfer problems.

Keywords: Optimal Homotopy Asymptotic Method; boundary layer flow; viscous fluid flow; heat transfer; exponential stretching sheet

MSC: 65L60; 76A10; 76D10; 76D05; 76M55

Citation: Ene, R.-D.; Pop, N.; Badarau, R. Heat and Mass Transfer Analysis for Viscous Fluid Flow: Dual Approximate Solutions. *Mathematics* **2023**, *11*, 1648. https://doi.org/10.3390/math11071648

Academic Editor: Ramoshweu Solomon Lebelo

Received: 15 February 2023
Revised: 11 March 2023
Accepted: 20 March 2023
Published: 29 March 2023

1. Introduction

Boundary layer behaviour over a moving continuous solid surface can be observed in many important technological processes and involves thermal effects, which show the characteristics of non-Newtonian fluids.

An important effect is viscous dissipation when the velocity gradient is high. The analysis of the temperature field as modified by the generation or absorption of heat in moving fluids is relevant for some physical problems, as presented by Sparrow and Cess [1], Topper [2], and Khashi et al. [3]. Further, the contributions of the suction parameter, Prandtl number, the heat source/sink parameter and the Eckert number to the heat transfer characteristics are found to be quite significant in [4].

In recent years, many the analytical methods have attempted to provide the solutions of different nonlinear models involving thermal effects.

Xu [5] analytically solved the mixed convection flow of a hybrid nanofluid in an inclined channel with top wall-slip due to wall stripe and constant heat flux conditions. Hayat et al. [6] analytically examined the melting phenomenon in the two-dimensional (2D) flow of fourth-grade material over a stretching surface, while taking into account the

existence of the Cattaneo–Christov (C-C) heat flux. The heat and mass transfer characteristics for a self-similarity boundary layer of an exponentially stretching surface were investigated by [7] using the Homotopy Analysis Method (HAM). This method is performed by several researchers, such as Khan et al. [8], Khan et al. [9], Khan et al. [10], Khan et al. [11], Zuhra et al. [12], Bilal et al. [13], and Shehzad et al. [14], who examine the thermal effect. Alizadeh et al. [15] solved the transient flow and heat transfer of a non-newtonian fluid (Casson fluid) between parallel disks in the presence of an external magnetic field semi-analytically using Least Square Method. Huaxing et al. [16] combined the effects of molecular and thermal diffusion processes by means of a generalized integral transform technique (GITT).

Some methods provide numerical solutions, such as those of Nadeem et al. [17], Abbasi et al. [18], Xie et al. [19], Abdelaziz et al. [20], Muhammad et al. [21], Mabood et al. [22], and Eid et al. [23], who numerically analyzed the flow and heat transfer resulting from an exponentially decreased sheet of hybrid nanoparticles, using the Runge–Kutta–Fehlberg method (RKF45) with the shooting technique. Boumaiza et al. [24] numerically investigated the effects of variable thermal conductivity in mixed convection in the presence of an external magnetic field using the Runge–Kutta–Fehlberg method (RKF) based on the shooting technique, and analytically by using the differential transform method (DTM). Gireesha et al. [25] numerically explored the thermal performance of a fully wet stretching/shrinking longitudinal fin with an exponential profile. Waini et al. [26] numerically solved the magnetohydrodynamic (MHD) mixed convection flow by considering thermal radiation. Tang et al. [27] applied some parallel finite element (FE) iterative methods for stationary incompressible magnetohydrodynamics (MHD).

For the analysis of many physical phenomena, numerical schemes or analytical/geometrical methods are applied in [28–35].

The Optimal Homotopy Asymptotic Method (OHAM) developed by Marinca et al. [36–41], and successfully applied to solve nonlinear equations arising in heat transfer [42–49], is used in the present paper to obtain effective and accurate dual analytic approximate solutions while taking into account the thermal effects.

The advantages of this procedure in comparison with HAM include the independence of small or large parameters, and the ease of optimally controlling the convergence of the approximate solutions.

Based on the mathematical model development in [7], in the present work, the OHAM technique is used to obtain effective and accurate dual analytic approximate solutions, while taking into account the thermal effects. Therefore, the novelty of our work is represented by the dual solutions of the mathematical model with the OHAM technique using only one iteration in comparison with [7], where only one solution is presented with the HAM method. Furthermore, ref. [7] did not elaborate on the possibility of dual solutions.

The paper is organized as follows: The Introduction is followed by a brief description of the two-dimensional flow of an incompressible viscous fluid passing a continuous stretching surface, taking into account the thermal effect. The steps of the OHAM technique are presented in Section 3. Section 4 presents the heat and mass transfer problem by the modified OHAM. Our results and some interesting behaviours of the effects of nonlinear stretching on flow and heat transfer characteristics are discussed in Section 5. The paper ends with conclusions.

2. Equations of Motion

In this section, the two-dimensional flow of an incompressible viscous fluid passes a continuous stretching surface in the half-plane, $y > 0$, taking into account the thermal effect. Additionally, the occurrence of the flow without suction/blowing and without partial slip is explored.

The schematic of the physical model is presented in Figure 1.

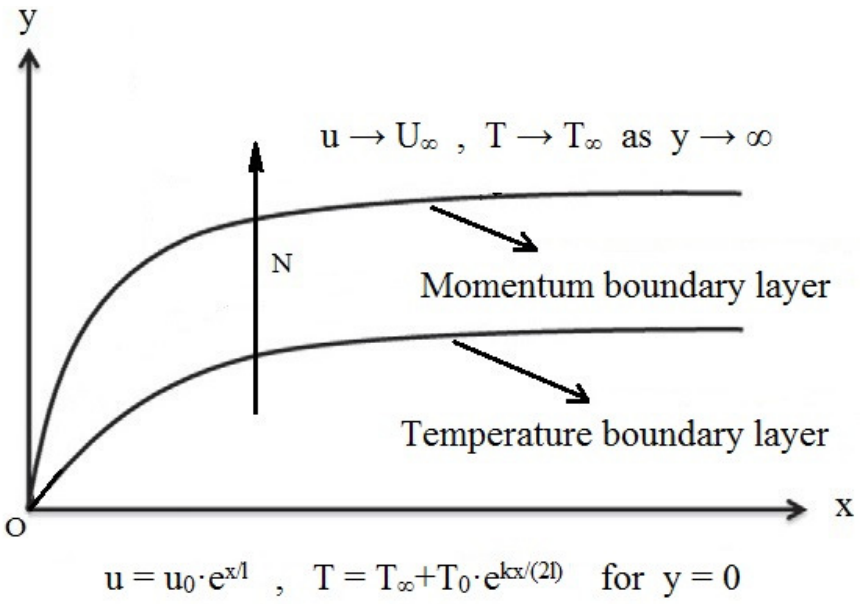

Figure 1. Schematic diagram of the physical model.

For the constant pressure at the boundary layer, the continuity, momentum and temperature equations governing the fluid flow are given by [7]:

$$\begin{aligned} &\frac{\partial u}{\partial x}+\frac{\partial v}{\partial y}=0, \\ &\rho\cdot\left(u\frac{\partial u}{\partial x}+v\frac{\partial u}{\partial y}\right)=\mu\frac{\partial^2 u}{\partial y^2}, \end{aligned} \tag{1}$$

$$u\frac{\partial T}{\partial x}+v\frac{\partial T}{\partial y}=\alpha\frac{\partial^2 T}{\partial y^2}\ . \tag{2}$$

The physical initial/boundary conditions can be written in the following form [7]:

$$\begin{aligned} &y=0\ :\ u=u_0\cdot e^{\frac{x}{l}}\ ,\ v=v_w\ ,\ T=T_\infty+T_0\cdot e^{\frac{k\cdot x}{2l}}, \\ &y\to\infty\ :\ u\to U_\infty\ ,\quad T\to T_\infty\ . \end{aligned} \tag{3}$$

By means of the similarity transformations,

$$\begin{aligned} &\eta=\sqrt{\tfrac{u_0\cdot\rho\cdot l}{2\mu}}\ \cdot\tfrac{y}{l}\cdot e^{(k\cdot x)/(2l)}\ ,\quad u=u_0e^{x/l}f'(\eta), \\ &v=-\tfrac{\mu}{\rho l}\cdot\sqrt{\tfrac{u_0\cdot\rho\cdot l}{2\mu}}\ \cdot e^{x/(2l)}[f(\eta)+\eta\cdot f'(\eta)], \\ &T=T_\infty+T_0\cdot e^{(k\cdot x)/(2l)}\theta(\eta) \end{aligned} \tag{4}$$

and by inserting Equation (4) into Equations (1)–(3), we obtain:

$$f'''+ff''-2\left(f'\right)^2=0, \tag{5}$$

$$\theta''+pr\left(f\theta'-k\cdot f'\theta\right)=0\ . \tag{6}$$

with the initial/boundary conditions:

$$\begin{aligned} &f(0) = 0\,, \quad f'(0) = 1\,, \quad \theta(0) = 1\,, \\ &f' \to 0\,, \quad \theta \to 0 \quad \text{for } \eta \to \infty, \end{aligned} \tag{7}$$

where the prime denotes differentiation with respect to η.

3. The Modified Optimal Homotopy Asymptotic Method (OHAM)

The steps of the modified OHAM technique [36] are presented in detail below:

(i) The nonlinear differential equation has the following general form:

$$\mathcal{L}_\varphi\Big(\varphi(\eta)\Big) + \mathcal{N}_\varphi\Big(\varphi(\eta)\Big) = 0, \tag{8}$$

under the boundary/initial conditions

$$\mathcal{B}_\varphi\Big(\varphi(\eta), \frac{d\varphi(\eta)}{d\eta}\Big) = 0, \tag{9}$$

where $\mathcal{L}_\varphi$ is an arbitrary linear operator, $\mathcal{N}_\varphi$ is the corresponding nonlinear operator and $\mathcal{B}_\varphi$ is an operator describing the boundary conditions.

(ii) The homotopic relation is given by:

$$\begin{aligned} &\mathcal{H}_\varphi\Big[\mathcal{L}_\varphi\Big(\varphi(\eta,p)\Big),\ H(\eta,C_i),\ \mathcal{N}_\varphi\Big(\varphi(\eta,p)\Big)\Big] = \\ &= \mathcal{L}_\varphi\Big(\varphi_0(\eta)\Big) + G_0(\eta) + p\Big[\mathcal{L}_\varphi\Big(\varphi_1(\eta,C_i)\Big) - H(\eta,C_i)\mathcal{N}_\varphi\Big(\varphi_0(\eta)\Big)\Big], \end{aligned} \tag{10}$$

where $G_0(\eta)$ is a given continuous function, $p \in [0,\ 1]$ is the embedding parameter and $H(\eta, C_i) \neq 0$ is an auxiliary convergence–control function depending on the variable η and of the convergence–control parameters $C_1, C_2, \ldots, C_s$, and choosing the unknown function $\varphi(\eta)$ in the following form:

$$\varphi(\eta, p) = \varphi_0(\eta) + p\varphi_1(\eta, C_i), \tag{11}$$

and by equating the coefficients of p^0 and p^1, respectively, we obtain:

- the zeroth-order deformation problem

$$\mathcal{L}_\varphi\Big(\varphi_0(\eta)\Big) + G_0(\eta) = 0, \quad \mathcal{B}_\varphi\Big(\varphi_0(\eta), \frac{d\varphi_0(\eta)}{d\eta}\Big) = 0, \tag{12}$$

- the first-order deformation problem

$$\begin{aligned} &\mathcal{L}_\varphi\Big(\varphi_1(\eta,C_i)\Big) = H(\eta,C_i)\mathcal{N}_\varphi\Big(\varphi_0(\eta)\Big), \\ &\mathcal{B}_\varphi\Big(\varphi_1(\eta,C_i), \tfrac{d\varphi_1(\eta,C_i)}{d\eta}\Big) = 0, \ \ i = 1,2,\ldots,s. \end{aligned} \tag{13}$$

(iii) $\varphi_0(\eta)$ could be obtained by solving the linear Equation (12).

(iv) In Equation (13), the expression $\mathcal{N}_\varphi$ has the following general form:

$$\mathcal{N}_\varphi(\varphi_0(\eta)) = \textstyle\sum_{i=1}^{n} h_i(\eta) g_i(\eta), \tag{14}$$

where n is a positive integer, and $h_i(\eta)$ and $g_i(\eta)$ are known elementary functions that depend on $\varphi_0(\eta)$ and on $\mathcal{N}_\varphi$.

The Equation (13) is a non-homogenous differential equation.
By means of the general theory of the differential equations, the computation of the function $\varphi_1(\eta, C_i)$ has the following form:

$$\varphi_1(\eta, C_i) = \sum_{i=1}^{m} H_i(\eta, h_j(\eta), C_j) g_i(\eta), \quad j = 1, \ldots, s, \tag{15}$$

or

$$\begin{aligned} &\varphi_1(\eta, C_i) = \sum_{i=1}^{m} H_i(\eta, g_j(\eta), C_j) h_i(\eta), \quad j = 1, \ldots, s, \\ &\mathcal{B}_\varphi\left(\varphi_1(\eta, C_i), \frac{d\varphi_1(\eta, C_i)}{d\eta}\right) = 0\,, \end{aligned} \tag{16}$$

where $m \in \mathbf{N}^*$ is an arbitrary number.
The above expressions of $H_i(\eta, h_j(\eta), C_j)$ contain linear combinations of the elementary functions h_j, $j = 1, \ldots, s$ and the parameters C_j, $j = 1, \ldots, s$.

(v) By means of Equation (11) for $p = 1$, the first-order analytical approximate solution of Equations (8) and (9), namely the OHAM-solution, is:

$$\overline{\varphi}(\eta, C_i) = \varphi(\eta, 1) = \varphi_0(\eta) + \varphi_1(\eta, C_i). \tag{17}$$

The parameters $C_1, C_2, \ldots, C_s$ can be optimally identified by means of various methods, such as the Galerkin method, the collocation method, the Kantorowich method, the least square method or the weighted residual method.
Thus, the first-order approximate solution (17) is well-determined.

4. Heat and Mass Transfer Problem

Based on a previous paper [50], the dual approximate solutions $\bar{f}(\eta)$ for Equation (5) are established.
The skin-friction coefficient is $\bar{f}''(0) = -1.2818085481$ for the first solution and $\bar{f}''(0) = -1.2916563038$ for the corresponding dual solution, respectively.
Using the same modified OHAM procedure, the approximate solutions, denoted by $\bar{\theta}$ of Equations (6) and (7) (for the unknown function θ), were obtained.
The expression of the linear operator $L_\theta(\eta)$ could be:

$$L_\theta(\eta) = \theta'' + K_1\theta', \tag{18}$$

where $K_1 > 0$ is an unknown parameter at this moment.
From Equation (6), the nonlinear operator N_θ corresponding to the unknown function θ becomes:

$$N_\theta(\eta) = -K_1\theta' + pr\left(f\theta' - k \cdot f'\theta\right). \tag{19}$$

There are a number of possibilities to choose from for the known function $G_0(\eta)$, including the following:

$$G_0(\eta) = (a_0 + a_1\eta + a_2\eta^2) \cdot e^{-K_2\eta}, \tag{20}$$

or

$$G_0(\eta) = (a_0 + a_1\eta + a_2\eta^2 + a_3\eta^3) \cdot e^{-K_2\eta},$$

or

$$G_0(\eta) = (a_0 + a_1\eta) \cdot e^{-K_2\eta} + (b_0 + b_1\eta + b_2\eta^2) \cdot e^{-2\cdot K_2\eta},$$

or

$$G_0(\eta) = (a_0 + a_1\eta + a_2\eta^2) \cdot e^{-K_2\eta} + (b_0 + b_1\eta + b_2\eta^2) \cdot e^{-K_3\eta},$$

and so on.

4.1. The Zeroth-Order Deformation Problem

Choosing for $G(\eta)$ the expression given by Equation (20), Equation (12) becomes:

$$\theta_0'' + K_1\theta_0' + (a_0 + a_1\eta + a_2\eta^2)\cdot e^{-K_2\eta} = 0, \quad \theta_0(0) = 1, \quad \theta_0(\infty) = 0 \tag{21}$$

with the solution

$$\theta_0(\eta) = (1 - b_0)e^{-K_1\eta} + (b_0 + b_1\eta + b_2\eta^2)\cdot e^{-K_2\eta}, \tag{22}$$

where b_0, b_1, b_2 depend on a_0, a_1, a_2, K_1, K_2 and will be optimally identified.

4.2. The First-Order Deformation Problem

Taking into account the function $\theta_0(\eta)$ (22), the nonlinear operator $N_{\theta_0}(\eta)$ from Equation (19) is:

$$\begin{aligned} &N_{\theta_0}(\eta) = m_0e^{-K_1\eta} + m_1e^{-(K+K_1)\eta} + \\ &+(n_0 + n_1\eta + n_2\eta^2)\cdot e^{-K_2\eta} + (p_0 + p_1\eta + p_2\eta^2)\cdot e^{-(K+K_2)\eta}, \end{aligned} \tag{23}$$

where the unknown convergence-control parameters m_0, m_1, n_0, n_1, n_2, p_0, p_1, p_2, K_1, K_2 will be optimally identified and they depend on b_0, b_1, b_2, K ($K = -1.1041868797$, for the first solution and $K = -3.2611576654$, for the corresponding dual solution, respectively [50]) and the physical parameters pr, k, respectively.

The comparison between the Equations (14) and (23) yields:

$$\begin{aligned} h_1^*(\eta) &= m_0, & g_1^*(\eta) &= e^{-K_1\eta}, \\ h_2^*(\eta) &= m_1, & g_2^*(\eta) &= e^{-(K+K_1)\eta}, \\ h_3^*(\eta) &= n_0 + n_1\eta + n_2\eta^2, & g_3^*(\eta) &= e^{-K_2\eta}, \\ h_4^*(\eta) &= p_0 + p_1\eta + p_2\eta^2, & g_4^*(\eta) &= e^{-(K+K_2)\eta}. \end{aligned} \tag{24}$$

For the first-order deformation problem given by Equation (13), the first approximation $\theta_1(\eta, D_i)$, from Equation (15), becomes:

$$\begin{aligned} &\theta_1(\eta, D_i) = H_1^*(\eta, D_i)e^{-K_1\eta} + H_2^*(\eta, D_i)e^{-(K+K_1)\eta} + \\ &+H_3^*(\eta, D_i)e^{-K_2\eta} + H_4^*(\eta, D_i)e^{-(K+K_2)\eta}, \end{aligned} \tag{25}$$

where D_i are the unknown real numbers and the unknown auxiliary functions $H_1^*(\eta, D_i)$, $\ldots$, $H_4^*(\eta, D_i)$ could be written in the form:

$$\begin{aligned} &H_1^*(\eta, D_i) = D_0\eta, \quad H_2^*(\eta, D_i) = D_7, \quad H_3^*(\eta, D_i) = D_1 + D_2\eta + D_3\eta^2, \\ &H_4^*(\eta, D_i) = D_4 + D_5\eta + D_6\eta^2, \end{aligned} \tag{26}$$

where $D_7 = -D_1 - D_4$.

Substituting Equation (26) into Equation (25) one can obtain:

$$\begin{aligned} &\theta_1(\eta, D_i) = D_0\eta e^{-K_1\eta} + D_7e^{-(K+K_1)\eta} + \\ &+(D_1 + D_2\eta + D_3\eta^2)e^{-K_2\eta} + (D_4 + D_5\eta + D_6\eta^2)e^{-(K+K_2)\eta}. \end{aligned} \tag{27}$$

4.3. The First-Order Analytical Approximate Solution $\bar{\theta}$

From Equations (22) and (27) the first-order approximate solution given by Equation (17) is obtained:

$$\begin{aligned}\bar{\theta}(\eta, D_i) = \theta_0(\eta) + \theta_1(\eta, D_i) = (1 - b_0 + D_0\eta)e^{-K_1\eta} + D_7 e^{-(K+K_1)\eta} + \\ + \left[b_0 + D_1 + (b_1 + D_2)\eta + (b_2 + D_3)\eta^2\right]e^{-K_2\eta} + (D_4 + D_5\eta + D_6\eta^2)e^{-(K+K_2)\eta}.\end{aligned} \tag{28}$$

5. Results and Discussion

The accuracy of the obtained results is shown by comparison of the above obtained approximate solutions with the corresponding numerical integration results, computed by means of the shooting method combined with the fourth-order Runge-Kutta method using Wolfram Mathematica 9.0 software. The goal of this section is to compute the convergence-control parameters K_1, K_2, b_0, b_1, b_2 and D_i, which appear in Equation (28), by the least square method for different values of the known parameters k and pr.

For fixed value of the parameter k and different values of the Prandtl number pr, four approximate solutions $\bar{\theta}(\eta)$ for temperature obtained from Equation (28), are presented below:

(a_1) the parameter $k = 0.25$, the Prandtl number $pr = 0.5$.

The first-order approximate solution is:

$$\begin{aligned}\bar{\theta}(\eta) = 6.4270002120 \cdot e^{-0.5270407713\cdot\eta} + (1 + 1.0977591304 \cdot \eta) \cdot e^{-1.6312276511\cdot\eta} + \\ + (-0.4903842473 - 0.8677675300 \cdot \eta - 0.0655183831 \cdot \eta^2) \cdot e^{-1.7700844051\cdot\eta} + \\ + (-5.6792005322 - 0.5323882885 \cdot \eta - 0.0584055951 \cdot \eta^2) \cdot e^{-0.6658975254\cdot\eta} + \\ + (-0.2574154323 - 0.1860126005 \cdot \eta - 0.0354344370 \cdot \eta^2) \cdot e^{-1.7700844051\cdot\eta}\end{aligned} \tag{29}$$

and the corresponding dual approximate solution becomes:

$$\begin{aligned}\bar{\theta}(\eta) = 0.4203972946 \cdot e^{-0.1531387065\cdot\eta} + (1 + 0.0224661936 \cdot \eta) \cdot e^{-1.2573255862\cdot\eta} + \\ + (-0.1188278766 - 0.1003865016 \cdot \eta - 0.0318369145 \cdot \eta^2) \cdot e^{-3.1410563458\cdot\eta} + \\ + (-0.8375405893 - 0.3581935944 \cdot \eta - 0.0048598683 \cdot \eta^2) \cdot e^{-1.5705281729\cdot\eta} + \\ + (0.5359711713 - 0.0282283101 \cdot \eta + 0.0012582354 \cdot \eta^2) \cdot e^{-0.4663412931\cdot\eta}.\end{aligned} \tag{30}$$

Other cases (a_2–a_6) for different values of the physical parameters k and pr are treated in Appendix A.

Tables 1 and 2 provides a comparison between the OHAM approximate solutions $\bar{\theta}_{OHAM}$ (temperature) given by Equations (29), (A1) and (A3) for the first solution, and the corresponding dual approximate solutions $\bar{\theta}_{OHAM}$ (temperature) given by Equations (30), (A2) and (A4), and numerical results for $k = 0.15$ for different values of the Prandtl number pr.

In Tables 3 and 4, respectively, the effect of the mass transfer coefficient $\theta'(0)$ obtained from Equations (29), (A1), (A3) and (A5) for both approximate solutions $\bar{\theta}(\eta)$ and corresponding numerical values are presented.

In the case of the approximate solution $\bar{\theta}(\eta)$ given by Equation (28), the residual from Equation (6) becomes:

$$R_{\bar{\theta}}(\eta) = \bar{\theta}''(\eta) + pr \cdot \left(\bar{f}(\eta)\bar{\theta}'(\eta) - k \cdot \bar{f}'(\eta)\bar{\theta}(\eta)\right). \tag{31}$$

The numerical values of the integral of the square residual given by Equation (31) are shown in Table 5.

Table 1. Comparison between the first-order approximate solutions $\bar{\theta}$ given by Equations (29), (A1) and (A3) and the corresponding numerical results for $k = 0.25$ and different values of the Prandtl parameter pr (absolute errors: $\epsilon_\theta = |\theta_{numerical} - \bar{\theta}_{OHAM}|$).

	$pr = 0.5$	$pr = 1$	$pr = 2.5$
η	$\theta_{numerical}$	$\theta_{numerical}$	$\theta_{numerical}$
0	1	1	1.
7/10	0.7489771062	0.6049297342	0.3645655020
7/5	0.5542053824	0.3451592660	0.1026555405
14/5	0.2979176957	0.1031937444	0.0055540922
7/2	0.2175152070	0.0553624933	0.0011533541
21/5	0.1586233161	0.0295455695	0.0002005939
28/5	0.0842151436	0.0083554452	−0.000042451
7	0.0446648315	0.0023547811	−0.000052955
	$\bar{\theta}_{OHAM}$	$\bar{\theta}_{OHAM}$	$\bar{\theta}_{OHAM}$
η	given by Equation (29)	given by Equation (A1)	given by Equation (A3)
0	1	1	1
7/10	0.7489754987	0.6049296367	0.3645643475
7/5	0.5542074180	0.3451592418	0.1026577273
14/5	0.2979183855	0.1031938730	0.0055556103
7/2	0.2175209607	0.0553624331	0.0011544802
21/5	0.1586257234	0.0295454423	0.0001987361
28/5	0.0842093003	0.0083555208	−0.0000415991
7	0.0446671512	0.0023548325	−0.0000527572
	ϵ_θ	ϵ_θ	ϵ_θ
η	for Equation (29)	for Equation (A1)	for Equation (A3)
0	0	0	0
7/10	$1.607455882179920 \times 10^{-6}$	$9.742094708720117 \times 10^{-8}$	$1.154538486203282 \times 10^{-6}$
7/5	$2.035591219806676 \times 10^{-6}$	$2.419851896640068 \times 10^{-8}$	$2.186829855102545 \times 10^{-6}$
14/5	$6.897985110887461 \times 10^{-7}$	$1.286033818881371 \times 10^{-7}$	$1.518143775084551 \times 10^{-6}$
7/2	$5.753703639754804 \times 10^{-6}$	$6.013523504849738 \times 10^{-8}$	$1.126029875720986 \times 10^{-6}$
21/5	$2.407287287453652 \times 10^{-6}$	$1.271883639693272 \times 10^{-7}$	$1.857745851002750 \times 10^{-6}$
28/5	$5.843302489164093 \times 10^{-6}$	$7.561148052809274 \times 10^{-8}$	$8.526737934899268 \times 10^{-7}$
7	$2.319736837258501 \times 10^{-6}$	$5.142016535871277 \times 10^{-8}$	$1.977883636694968 \times 10^{-7}$

Table 2. Comparison between the corresponding dual approximate solutions $\bar{\theta}$ given by Equations (30), (A2) and (A4) and the corresponding numerical results for $k = 0.25$ and different values of the Prandtl parameter pr (absolute errors: $\epsilon_\theta = |\theta_{numerical} - \bar{\theta}_{OHAM}|$).

	$pr = 0.5$	$pr = 1$	$pr = 2.5$
η	$\theta_{numerical}$	$\theta_{numerical}$	$\theta_{numerical}$
0	1	1	1
7/10	0.7858094356	0.6190556769	0.3688458421
7/5	0.6228249648	0.3691930827	0.1074930546
14/5	0.4085135781	0.1323390363	0.0072619140
7/2	0.3388566718	0.0822984147	0.0019692645
21/5	0.2852286001	0.0530118448	0.0006029330
28/5	0.2095004124	0.0244710236	0.0001201557
7	0.1593196243	0.0127723199	0.0000713911

Table 2. *Cont.*

	$\bar{\theta}_{OHAM}$	$\bar{\theta}_{OHAM}$	$\bar{\theta}_{OHAM}$
η	given by Equation (30)	given by Equation (A2)	given by Equation (A4)
0	1	1	1
7/10	0.7858136455	0.6190546849	0.3688476879
7/5	0.6228223796	0.3691937408	0.1074929959
14/5	0.4085152511	0.1323390010	0.0072605998
7/2	0.3388541904	0.0822992211	0.0019705677
21/5	0.2852266049	0.0530118072	0.0006039728
28/5	0.2095026184	0.0244705609	0.0001187666
7	0.1593190414	0.0127728948	0.0000719311
	ϵ_θ	ϵ_θ	ϵ_θ
η	for Equation (30)	for Equation (A2)	for Equation (A4)
0	0	0	0
7/10	$4.209839553404038 \times 10^{-6}$	$9.919631346333446 \times 10^{-7}$	$1.845765404961952 \times 10^{-6}$
7/5	$2.585204789018469 \times 10^{-6}$	$6.580974769021530 \times 10^{-7}$	$5.869076206976853 \times 10^{-8}$
14/5	$1.673009802138914 \times 10^{-6}$	$3.525957825711856 \times 10^{-8}$	$1.314288065634369 \times 10^{-6}$
7/2	$2.481370770357482 \times 10^{-6}$	$8.064145169128789 \times 10^{-7}$	$1.303131223448148 \times 10^{-6}$
21/5	$1.995245388297650 \times 10^{-6}$	$3.768198066078643 \times 10^{-8}$	$1.039826044727616 \times 10^{-6}$
28/5	$2.205963331475269 \times 10^{-6}$	$4.627662200211435 \times 10^{-7}$	$1.389042267445562 \times 10^{-6}$
7	$5.828584578315699 \times 10^{-7}$	$5.749493005424017 \times 10^{-7}$	$5.400103917853105 \times 10^{-7}$

Table 3. Comparison between the heat transfer coefficient $\bar{\theta}'(0)$ obtained by means of the OHAM for different values of the Prandtl number pr and the parameter k, respectively, in the case of the first-order approximate solution.

		Numerical Solution	**OHAM Solution**	**Absolute Errors**
pr	k	$\theta'_{numerical}(0)$	$\bar{\theta}'_{OHAM}(0)$	$\epsilon_{\theta'(0)} = \lvert\theta'_{numerical}(0) - \bar{\theta}'_{OHAM}(0)\rvert$
0.5	0.15	−0.3727417350	−0.3727417250	$1.000000127149292 \times 10^{-8}$
0.5	0.25	−0.4014940569	−0.4014939569	$9.999999639465074 \times 10^{-8}$
0.5	0.5	−0.4686586964	−0.4686585964	$9.999899136525770 \times 10^{-8}$
1	0.15	−0.6171741875	−0.6171740875	$9.999999328602627 \times 10^{-8}$
1	0.25	−0.6608537627	−0.6608537527	$1.000000671158574 \times 10^{-8}$
1	0.5	−0.7647932545	−0.7647931545	$9.999999373011548 \times 10^{-8}$
2.5	0.15	−1.1185512466	−1.1185511466	$9.999999783794067 \times 10^{-8}$
2.5	0.25	−1.1923711840	−1.1923710840	$9.999999694976225 \times 10^{-8}$
2.5	0.5	−1.3666535048	−1.3666534948	$1.000000171558213 \times 10^{-8}$

Table 4. Comparison between the heat transfer coefficient $\bar{\theta}'(0)$ obtained by means of the OHAM for different values of the Prandtl number pr and the parameter k, respectively, in the case of the corresponding dual approximate solution.

		Numerical Solution	**OHAM Solution**	**Absolute Errors**
pr	k	$\theta'_{numerical}(0)$	$\bar{\theta}'_{OHAM}(0)$	$\epsilon_{\theta'(0)}$
0.5	0.15	−0.3238611974	−0.3238611874	$1.000000138251522 \times 10^{-8}$
0.5	0.25	−0.3473663384	−0.3473662384	$9.999999683873995 \times 10^{-8}$
0.5	0.5	−0.4014554630	−0.4014554530	$1.000000332540551 \times 10^{-8}$

Table 4. *Cont.*

		Numerical Solution	OHAM Solution	Absolute Errors
pr	k	$\theta'_{numerical}(0)$	$\bar{\theta}'_{OHAM}(0)$	$\epsilon_{\theta'(0)}$
1	0.15	−0.5929179987	−0.5929179887	$9.999954753148188 \times 10^{-9}$
1	0.25	−0.6393617637	−0.6393617537	$9.999972516716582 \times 10^{-9}$
1	0.5	−0.7402284508	−0.7402283508	$9.999999661669534 \times 10^{-8}$
2.5	0.15	−1.1110208487	−1.1110208387	$1.000000215967134 \times 10^{-8}$
2.5	0.25	−1.1848129415	−1.1848129315	$1.000000104944831 \times 10^{-8}$
2.5	0.5	−1.3591246415	−1.3591246315	$1.000000637851883 \times 10^{-8}$

Table 5. Integral of the square residual given by Equation (31) respectively, for different values of the parameters k and pr.

		The First Solution	The Corresponding Dual Solution
k	pr	$\int_0^\infty R_{\bar{\theta}}^2(\eta)\, d\eta$	$\int_0^\infty R_{\bar{\theta}}^2(\eta)\, d\eta$
0.15	0.5	$6.575432601542083 \times 10^{-9}$	$2.908978433213571 \times 10^{-10}$
0.25	0.5	$2.692683749426807 \times 10^{-8}$	$6.130825386312505 \times 10^{-8}$
0.5	0.5	$2.877470397657074 \times 10^{-10}$	$2.329753093802392 \times 10^{-7}$
0.15	1	$4.686687280794850 \times 10^{-9}$	$4.935777384019864 \times 10^{-8}$
0.25	1	$2.769513856968707 \times 10^{-10}$	$3.168740967468855 \times 10^{-9}$
0.5	1	$1.390428703762422 \times 10^{-9}$	$9.337205151229265 \times 10^{-6}$
0.15	2.5	$2.424695938193004 \times 10^{-6}$	$1.109703562037575 \times 10^{-6}$
0.25	2.5	$2.547691207587611 \times 10^{-7}$	$8.786794816590718 \times 10^{-8}$
0.5	2.5	$3.953512700816478 \times 10^{-10}$	$5.589488626508835 \times 10^{-6}$

5.1. Influence of the Prandtl Number pr

From Figures 2–5 we can notice that the variation of the temperature $\bar{\theta}(\eta)$ decreases with the increasing of the Prandtl number pr, for some fixed values of the parameter k.

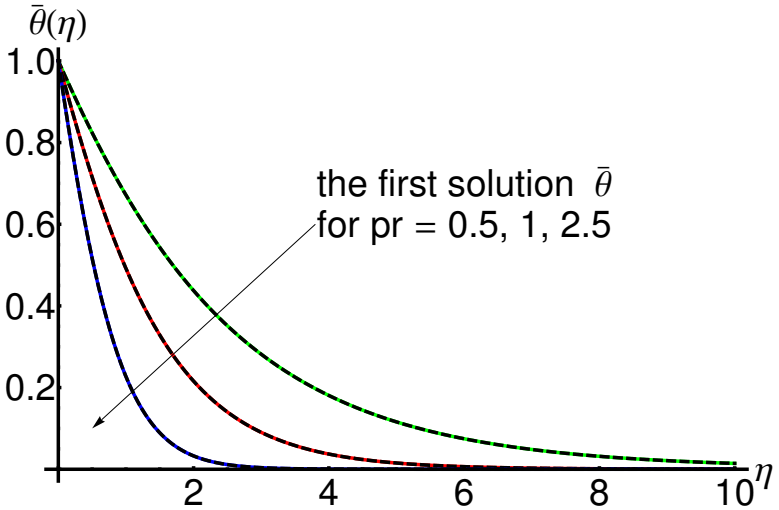

Figure 2. Variation of the temperature $\bar{\theta}(\eta)$ given by Equations (29), (A1) and (A3) with the Prandtl number $pr = 0.5,\ 1,\ 2.5$ for $k = 0.15$: OHAM solution (with lines) and numerical solution (dashing lines), respectively.

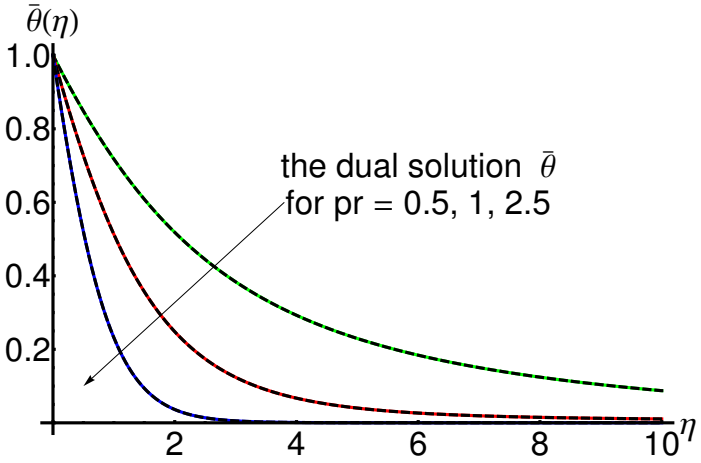

Figure 3. Variation of the temperature $\bar{\theta}(\eta)$ given by Equations (30), (A2) and (A4) with the Prandtl number $pr = 0.5,\ 1,\ 2.5$ for $k = 0.15$: OHAM solution (with lines) and numerical solution (dashing lines), respectively.

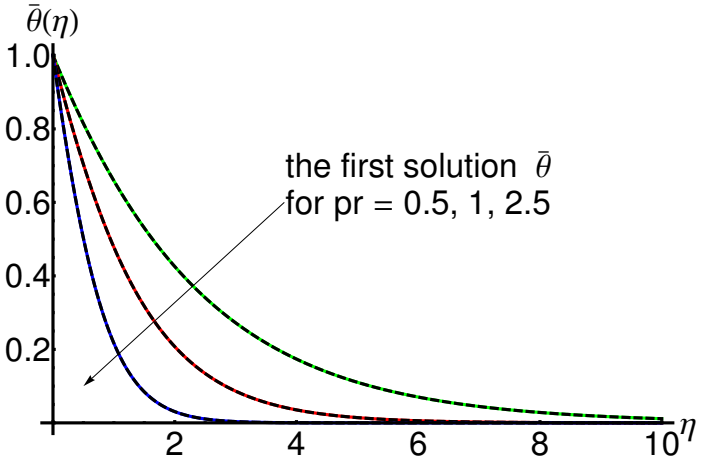

Figure 4. Variation of the temperature $\bar{\theta}(\eta)$ given by Equations (29), (A1) and (A3) with the Prandtl number $pr = 0.5,\ 1,\ 2.5$ for $k = 0.25$: OHAM solution (with lines) and numerical solution (dashing lines), respectively.

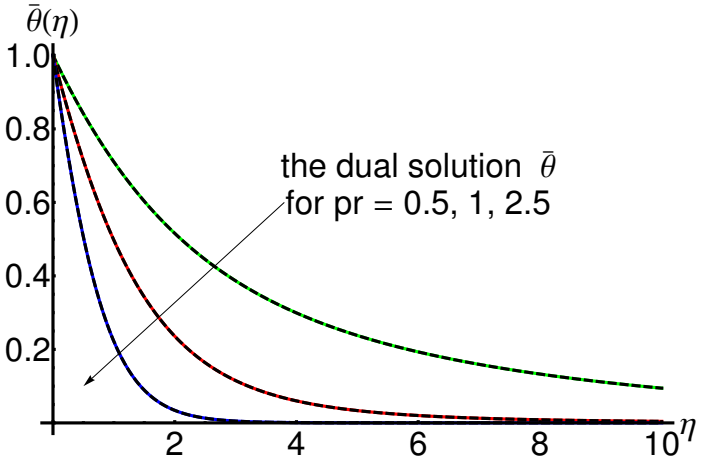

Figure 5. Variation of the temperature $\bar{\theta}(\eta)$ given by Equations (30), (A2) and (A4) with the Prandtl number $pr = 0.5,\ 1,\ 2.5$ for $k = 0.25$: OHAM solution (with lines) and numerical solution (dashing lines), respectively.

5.2. Influence of the Temperature Distribution Parameter k

Additionally, Figures 6 and 7 show that the variation of the temperature $\bar{\theta}(\eta)$ decreases with the increase in the parameter k for some fixed values of the Prandtl number pr.

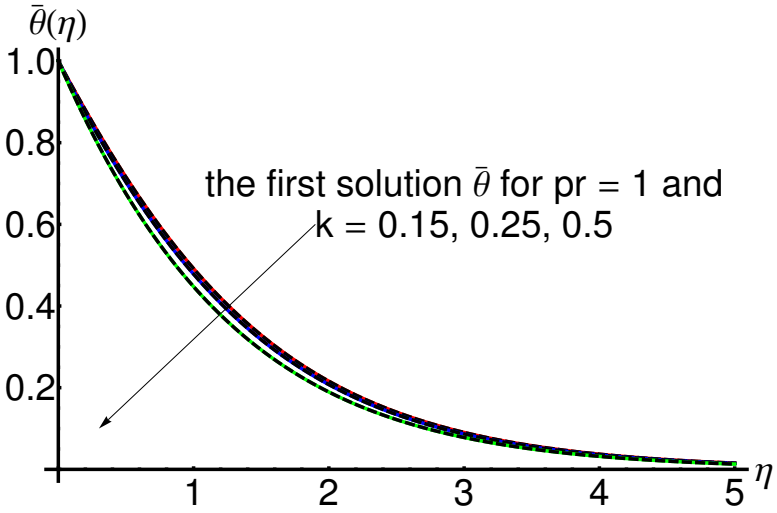

Figure 6. Variation of the temperature $\bar{\theta}(\eta)$ given by Equations (A1), (A7) and (A9) with the parameter $k = 0.15,\ 0.25,\ 0.5$ for $pr = 1$: OHAM solution (with lines) and numerical solution (dashed lines), respectively.

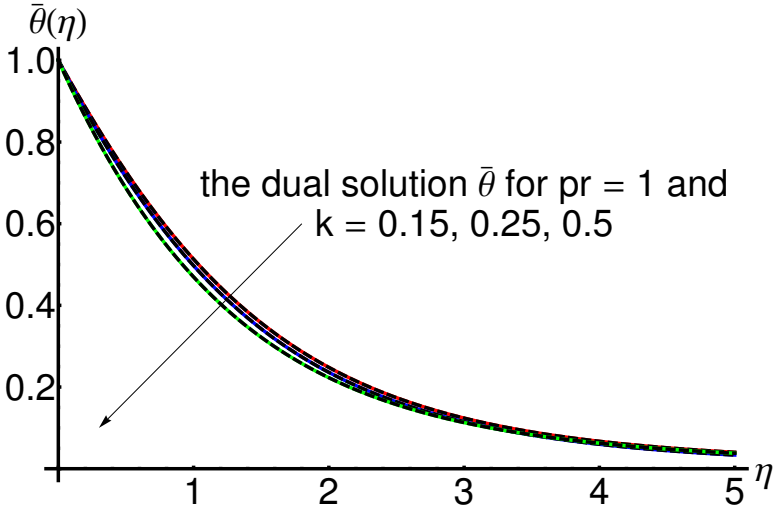

Figure 7. Variation of the temperature $\bar{\theta}(\eta)$ given by Equations (A2), (A8) and (A10) with the parameter $k = 0.15,\ 0.25,\ 0.5$ for $pr = 1$: OHAM solution (with lines) and numerical solution (dashed lines), respectively.

From all the Tables 1–5 and Figures 2–7 we can summarize that the OHAM solutions are effective and very accurate.

The advantages of the modified OHAM technique by comparison of the OHAM-solutions with the corresponding iterative solutions obtained by means of the iterative method developed in [51] are presented below.

The Equations (5) and (6) convert in the following system:

$$\begin{cases} f_1'(\eta) = f_2(\eta) \\ f_2'(\eta) = f_3(\eta) \\ f_3'(\eta) = 2f_2^2(\eta) - f_1(\eta)f_3(\eta) \\ \theta_1'(\eta) = \theta_2(\eta) \\ \theta_2'(\eta) = pr \cdot \Big(k \cdot f_2(\eta)\theta_1(\eta) - f_1(\eta)\theta_2(\eta)\Big) \end{cases}, \tag{32}$$

where $f_1(\eta) = f(\eta)$, $f_2(\eta) = f'(\eta)$, $f_3(\eta) = f''(\eta)$, $\theta_1(\eta) = \theta(\eta)$, $\theta_2(\eta) = \theta'(\eta)$.

By integration of the system (32) over the interval $[0,\ \eta]$, the following expressions are obtained:

$$\begin{aligned} f_1(\eta) &= f_1(0) + \int_0^\eta f_2(s)\, ds \\ f_2(\eta) &= f_2(0) + \int_0^\eta f_3(s)\, ds \\ f_3(\eta) &= f_3(0) + \int_0^\eta \Big(2f_2^2(s) - f_1(s)f_3(s)\Big)\, ds \\ \theta_1(\eta) &= \theta_1(0) + \int_0^\eta \theta_2(s)\, ds \\ \theta_2(\eta) &= \theta_2(0) + \int_0^\eta pr \cdot \Big(k \cdot f_2(s)\theta_1(s) - f_1(s)\theta_2(s)\Big)\, ds \end{aligned} . \tag{33}$$

The iterative algorithm is written as:

$$\begin{aligned} &f_{1,0}(\eta) = f_1(0)\,, \quad f_{1,1}(\eta) = N_1(f_{1,0}, f_{2,0}, f_{3,0}, \theta_{1,0}, \theta_{2,0}) = \int_0^\eta f_{2,0}(s)\, ds\,, \\ &f_{2,0}(\eta) = f_2(0)\,, \quad f_{2,1}(\eta) = N_2(f_{1,0}, f_{2,0}, f_{3,0}, \theta_{1,0}, \theta_{2,0}) = \int_0^\eta f_{3,0}(s)\, ds\,, \\ &f_{3,0}(\eta) = f_3(0)\,, \quad f_{3,1}(\eta) = N_3(f_{1,0}, f_{2,0}, f_{3,0}, \theta_{1,0}, \theta_{2,0}) = \int_0^\eta \Big(2f_{2,0}^2(s) - f_{1,0}(s)f_{3,0}(s)\Big)\, ds\,, \\ &\theta_{1,0}(\eta) = \theta_1(0)\,, \quad \theta_{1,1}(\eta) = N_4(f_{1,0}, f_{2,0}, f_{3,0}, \theta_{1,0}, \theta_{2,0}) = \int_0^\eta \theta_{2,0}(s)\, ds\,, \\ &\theta_{2,0}(\eta) = \theta_2(0)\,, \quad \theta_{2,1}(\eta) = N_5(f_{1,0}, f_{2,0}, f_{3,0}, \theta_{1,0}, \theta_{2,0}) = \int_0^\eta pr \cdot \Big(k \cdot f_{2,0}(s)\theta_{1,0}(s) - f_{1,0}(s)\theta_{2,0}(s)\Big)\, ds\,, \\ &\ldots \\ &f_{1,m}(\eta) = N_1\left(\sum_{i=0}^{m-1} f_{1,i}, \sum_{i=0}^{m-1} f_{2,i}, \sum_{i=0}^{m-1} f_{3,i}, \sum_{i=0}^{m-1} \theta_{1,i}, \sum_{i=0}^{m-1} \theta_{2,i}\right) - N_1\left(\sum_{i=0}^{m-2} f_{1,i}, \sum_{i=0}^{m-2} f_{2,i}, \sum_{i=0}^{m-2} f_{3,i}, \sum_{i=0}^{m-2} \theta_{1,i}, \sum_{i=0}^{m-2} \theta_{2,i}\right), \\ &f_{2,m}(\eta) = N_2\left(\sum_{i=0}^{m-1} f_{1,i}, \sum_{i=0}^{m-1} f_{2,i}, \sum_{i=0}^{m-1} f_{3,i}, \sum_{i=0}^{m-1} \theta_{1,i}, \sum_{i=0}^{m-1} \theta_{2,i}\right) - N_2\left(\sum_{i=0}^{m-2} f_{1,i}, \sum_{i=0}^{m-2} f_{2,i}, \sum_{i=0}^{m-2} f_{3,i}, \sum_{i=0}^{m-2} \theta_{1,i}, \sum_{i=0}^{m-2} \theta_{2,i}\right), \\ &f_{3,m}(\eta) = N_3\left(\sum_{i=0}^{m-1} f_{1,i}, \sum_{i=0}^{m-1} f_{2,i}, \sum_{i=0}^{m-1} f_{3,i}, \sum_{i=0}^{m-1} \theta_{1,i}, \sum_{i=0}^{m-1} \theta_{2,i}\right) - N_3\left(\sum_{i=0}^{m-2} f_{1,i}, \sum_{i=0}^{m-2} f_{2,i}, \sum_{i=0}^{m-2} f_{3,i}, \sum_{i=0}^{m-2} \theta_{1,i}, \sum_{i=0}^{m-2} \theta_{2,i}\right), \\ &\theta_{1,m}(\eta) = N_4\left(\sum_{i=0}^{m-1} f_{1,i}, \sum_{i=0}^{m-1} f_{2,i}, \sum_{i=0}^{m-1} f_{3,i}, \sum_{i=0}^{m-1} \theta_{1,i}, \sum_{i=0}^{m-1} \theta_{2,i}\right) - N_4\left(\sum_{i=0}^{m-2} f_{1,i}, \sum_{i=0}^{m-2} f_{2,i}, \sum_{i=0}^{m-2} f_{3,i}, \sum_{i=0}^{m-2} \theta_{1,i}, \sum_{i=0}^{m-2} \theta_{2,i}\right), \\ &\theta_{2,m}(\eta) = N_5\left(\sum_{i=0}^{m-1} f_{1,i}, \sum_{i=0}^{m-1} f_{2,i}, \sum_{i=0}^{m-1} f_{3,i}, \sum_{i=0}^{m-1} \theta_{1,i}, \sum_{i=0}^{m-1} \theta_{2,i}\right) - N_5\left(\sum_{i=0}^{m-2} f_{1,i}, \sum_{i=0}^{m-2} f_{2,i}, \sum_{i=0}^{m-2} f_{3,i}, \sum_{i=0}^{m-2} \theta_{1,i}, \sum_{i=0}^{m-2} \theta_{2,i}\right), \\ &m \geq 2\,. \end{aligned} \tag{34}$$

By carrying out the iterative method, the solutions of the Equations (5) and (6) have the form:

$$f_{1_{iter}}(\eta) = \sum_{m=0}^{\infty} f_{1,m}(t)\ ,\ f_{2_{iter}}(\eta) = \sum_{m=0}^{\infty} f_{2,m}(\eta)\ ,\ f_{3_{iter}}(\eta) = \sum_{m=0}^{\infty} f_{3,m}(\eta)\ ,\ \theta_{1_{iter}}(\eta) = \sum_{m=0}^{\infty} \theta_{3,m}(\eta)\ ,\theta_{2_{iter}}(\eta) = \sum_{m=0}^{\infty} \theta_{2,m}(\eta)\ .$$

Using five iterations, with the initial conditions $f_1(0) = 0$, $f_2(0) = 1$, $f_3(0) = -1.2818085481$, $\theta_1(0) = 1$, $\theta_2(0) = -0.6608537627$ (presented in the Table 3) and the physical constants $k = 0.25$, $pr = 1$, taking into account of the algorithm (33), the iterative solutions become:

$$\begin{aligned} &f_{1_{iter}}(\eta) = \sum_{m=0}^{5} f_{1,m}(\eta) = \eta - 0.6409042740\eta^2 + 0.3333333333\eta^3 - 0.1602260685\eta^4 + \\ &+0.0744091621\eta^5 - 0.0160226068\eta^6 + 0.0016144588\eta^7 + 0.0008177037\eta^8\ , \\ &\theta_{1_{iter}}(\eta) = \sum_{m=0}^{5} \theta_{1,m}(\eta) = 1 - 0.6608537627\eta - 0.3304268813\eta^2 - 0.1101422937\eta^3 - \\ &-0.0275355734\eta^4 - 0.0055071146\eta^5\ . \end{aligned} \tag{35}$$

A comparison between the OHAM solutions $\bar{f}_{OHAM}$, $\bar{\theta}_{OHAM}$ and the corresponding iterative solutions $f_{1_{iter}}$, $\theta_{1_{iter}}$ given in Equation (35) is highlighted graphically in Figures 8 and 9 and tabularly in Table 6, respectively.

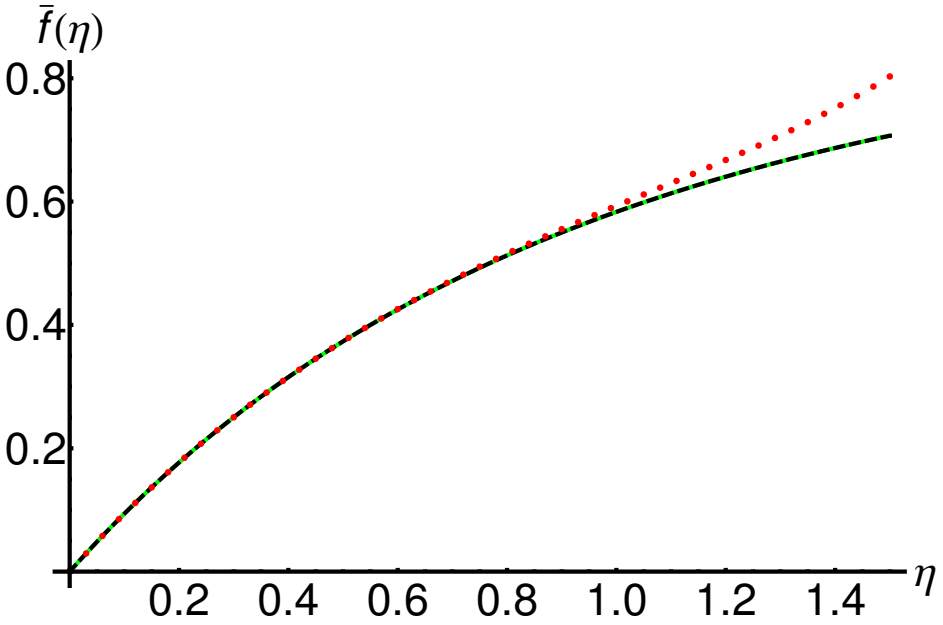

Figure 8. Comparison between the approximate analytical solution $\bar{f}(\eta)$, of the Equation (5) given by Equation [50], the iterative solution $f_{1_{iter}}(\eta)$ given by Equation (35) and the corresponding numerical solution: numerical solution (with lines), OHAM solution (dashed lines), and iterative solution (dotted curve), respectively.

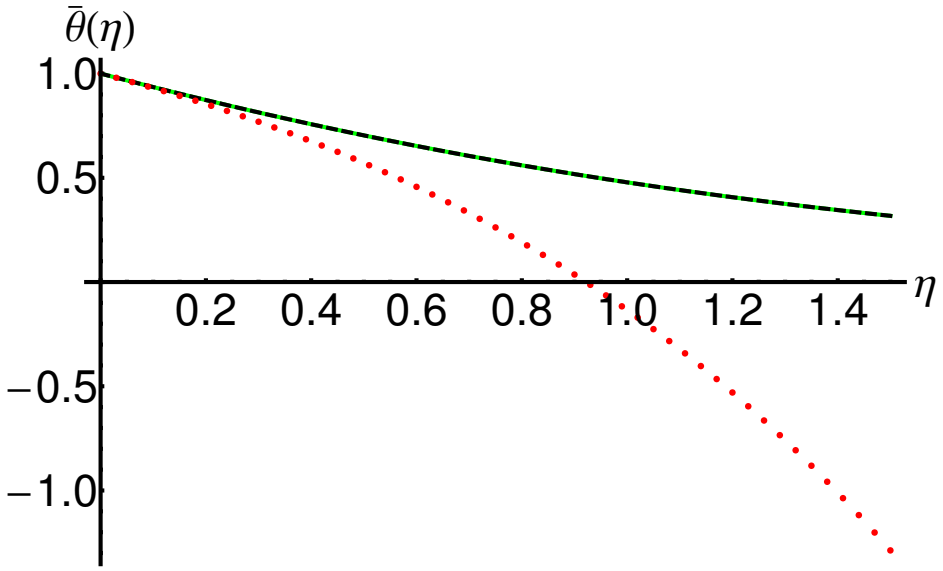

Figure 9. Comparison between the approximate analytical solution $\bar{\theta}(\eta)$, of the Equation (6) given by Equation (A1), the corresponding numerical solution and the iterative solution $\theta_{1_{iter}}(\eta)$ given by Equation (35): numerical solution (with lines), OHAM solution (dashed lines), and iterative solution (dotted curve), respectively.

The precision and efficiency of the OHAM method (using just one iteration) against to the iterative method described in [51] (using five iterations) arising from the presented comparison.

Table 6. Comparison between the approximate analytical solution $\bar{f}(\eta)$ given by Equation [50], the iterative solution $f_{1_{iter}}(\eta)$ given by Equation (35) and the corresponding numerical solution.

η	$f_{numerical}$	$\bar{f}_{OHAM}$ [50]	$f_{1_{iter}}$
0	0	0	0
1/10	0.0939089690	0.0939087919	0.0939089962
1/5	0.1767959477	0.1767950192	0.1767969422
3/10	0.2501798542	0.2501779276	0.2501903246
2/5	0.3153313350	0.3153286203	0.3153863643
1/2	0.3733200865	0.3733170634	0.3735172090
3/5	0.4250519374	0.4250491302	0.4256065973
7/10	0.4712981406	0.4712959627	0.4726209608
4/5	0.5127187008	0.5127173844	0.5155172621
9/10	0.5498810935	0.5498806830	0.5552901957
1	0.5832753856	0.5832757722	0.5930217087

Case Study

In the following we apply our analytical results in the case of the hydraulic oil with a large application at the hydraulic drive systems as turbines, pumps, naval propellers.

We consider the fluid flow scenario from a hydraulic installation with the following values of the characteristic quantities: the reference velocity $u_0 = 0.05$ [m/s], the reference temperature $T_0 = 40$, the kinematical viscosity $\nu = 46 \cdot 10^{-6}$ [m^2/s] and the environmental temperature $T_\infty = 22$, respectively.

The analytical obtained results in our paper using the specific physical sizes, are presented in Figures 10 and 11 for the first solution and in Figures 12 and 13 for the corresponding dual solution, respectively.

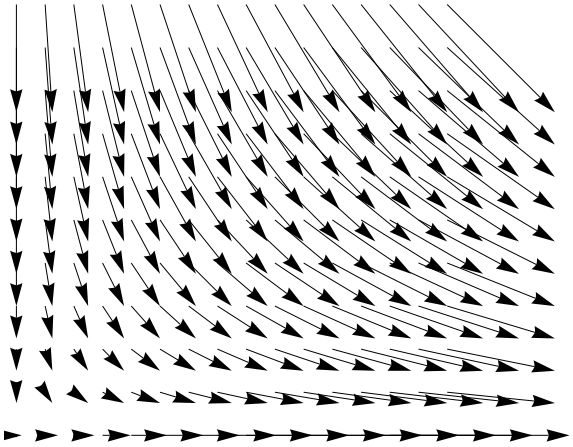

Figure 10. The vector field $(u,\ v)$ from Equation (4) for hydraulic oil at a temperature of 40 °C, in the case of the first-solution given by Equation [50].

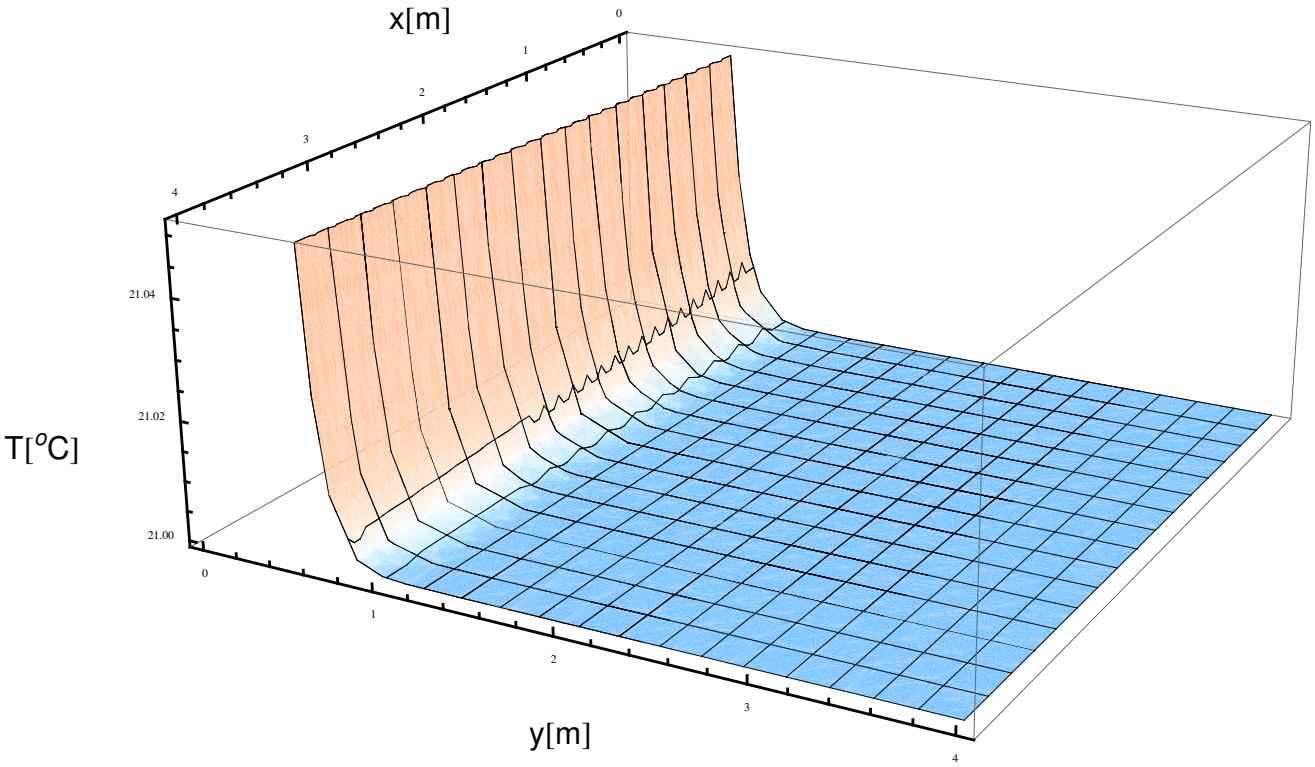

Figure 11. The 3D-profile of the temperature T from Equation (4) for $k = 0.25$, $pr = 1$ for hydraulic oil at a temperature of 40 °C, in the case of the first-solution given by Equation (A1).

The obtained results are in agreement with the Fluid Mechanics [52,53].

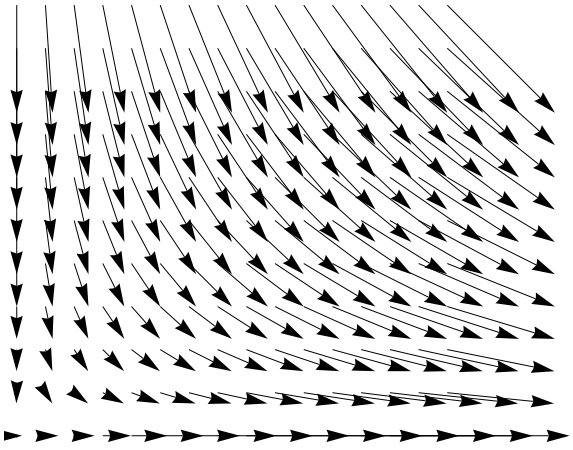

Figure 12. The vector field (u, v) from Equation (4) for hydraulic oil at a temperature of 40 °C, in the case of the corresponding dual solution given by Equation [50].

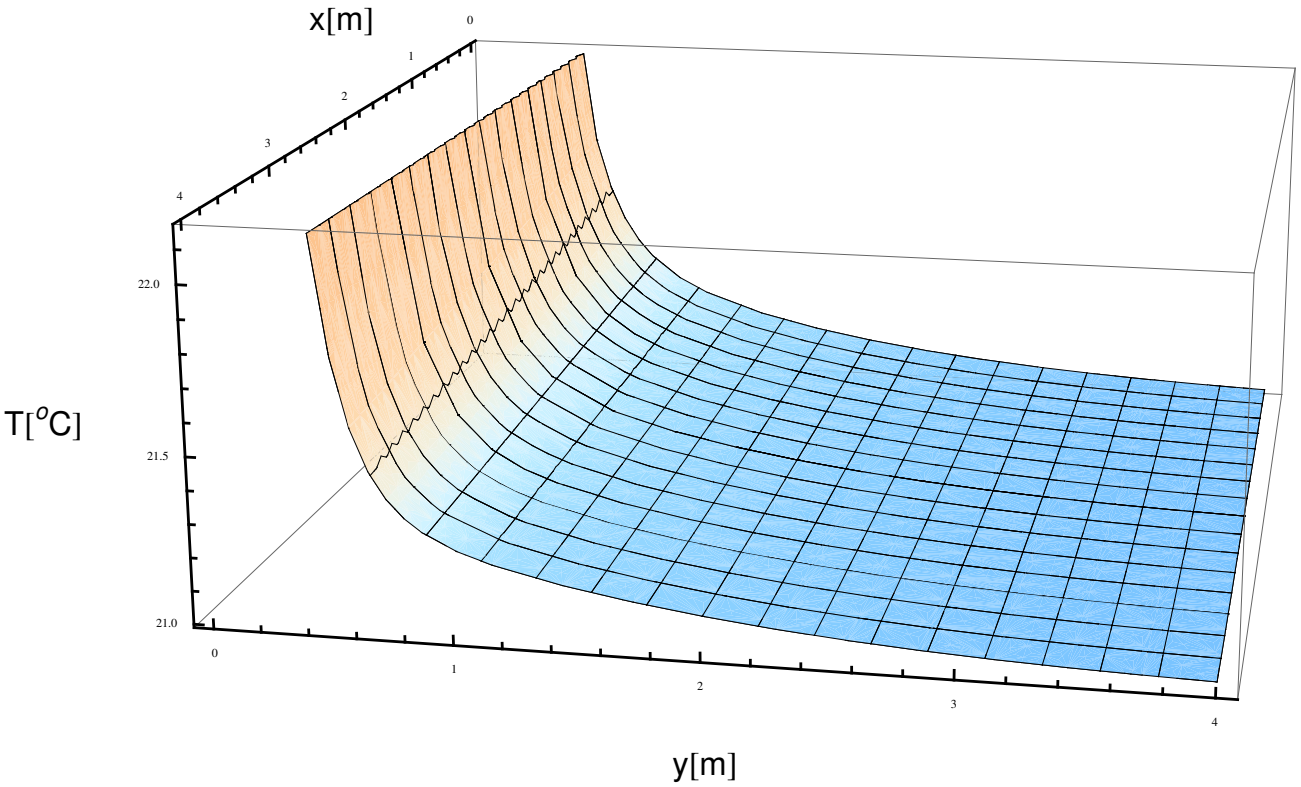

Figure 13. The 3D-profile of the temperature T from Equation (4) for $k = 0.25$, $pr = 1$ for hydraulic oil at a temperature of 40 °C, in the case of the corresponding dual solution given by Equation (A2).

6. Conclusions

The steady boundary layer flow and heat transfer over a stretching sheet were analyzed by using a nonlinear differential equation. The variation of the temperature $\theta(\eta)$ decreases with the increase in the Prandtl number pr for some fixed values of the parameter k. As a result, we can observe a decrease in the fluid temperature. This shows that more heat is released from the sheet and the Prandtl number decreases in the boundary layer thickness. Therefore, the heat transfer rate increases.

The processes with strongly nonlinear behaviors appear in different technological applications. Thus, an approximate analytical solution is a more realistic option.

The OHAM treatment related to the heat and mass transfer problem without partial slip in the flow of a viscous fluid over an exponentially stretching sheet without suction/blowing is considered and provides an accurate solution for the nonlinear differential equation with initial and boundary conditions.

In this paper, the thermal effects of the Prandtl number and the temperature distribution parameter are analytically analyzed. The variations of the dimensionless surface temperature and heat transfer characteristics with the governing parameters are graphed and tabulated. In particular, the analytically obtained results are applied from the hydraulic system.

The advantage of the method applied in this work is the efficiency by only one iteration. Other advantages, including accuracy, flexibility, validity and convergence, of the approximate solutions are highlighted by comparing the OHAM solutions with the corresponding iterative solutions.

Some characteristics of the heat and mass transfer, such as the vector field (u, v) and the temperature profile T are graphically depicted in a case study of the hydraulic oil using the obtained approximate solutions via OHAM.

This study is useful for many engineering applications of heat and mass transfer problems such as strand casting processes, polymeric liquids, the extraction of metals and polymers, glass-fiber production, and physiological fluid dynamics.

Author Contributions: Conceptualization, N.P.; data curation, R.-D.E. and N.P.; formal analysis, N.P.; investigation, R.-D.E. and R.B.; methodology, R.-D.E. and R.B.; software, R.-D.E.; supervision, N.P.; validation, R.-D.E. and N.P.; visualization, R.-D.E. and N.P.; writing—original draft, R.-D.E., R.B. and N.P. All authors have read and agreed to the published version of the manuscript.

Funding: This research received no external funding.

Institutional Review Board Statement: Not applicable.

Informed Consent Statement: Not applicable.

Data Availability Statement: Not applicable.

Conflicts of Interest: The authors declare no conflict of interest.

Nomenclature/Notation

Symbols	Names
$u,\ v$	Velocity components (m/s)
$x,\ y$	Cartesian coordinates (m)
ν	Kinematical viscosity (m^2/s)
μ	Viscosity
ρ	Fluid density
U_∞	Velocity of uniform flow
$u_0,\ T_0$	Reference velocity and reference temperature
N	Velocity slip factor
l	Characteristic length
pr	Prandtl number
k	Parameter of temperature distribution
T_∞	Environment temperature (K)
η	Independent dimensionless variable
$f(\eta)$	Stream function
$\theta(\eta)$	Temperature
OHAM solution	approximate analytical solution by means of the modified Optimal Homotopy Asymptotic Method

Appendix A

In this section there are presented in details the first-order approximate solution given by Equation (28) and the corresponding dual solution for different values of the physical parameters.

(a_2) the parameter $k = 0.25$, the Prandtl number $pr = 1$.

$$\begin{aligned}\bar{\theta}(\eta) &= 1.1600261597 \cdot e^{-0.9234397221\cdot\eta} + (1 - 0.3362966408 \cdot \eta)e^{-2.0276266018\cdot\eta} + \\ &+(-1.3520589334 + 0.2475145276 \cdot \eta - 0.0094831510 \cdot \eta^2)e^{-2.0138501698\cdot\eta} + \\ &+(0.1720819672 + 0.0218466525 \cdot \eta - 0.0001162030 \cdot \eta^2)e^{-0.9096632901\cdot\eta} + \\ &+(0.0199508065 + 0.0189709502 \cdot \eta + 0.0059452174 \cdot \eta^2)e^{-4.0277003397\cdot\eta}\end{aligned} \tag{A1}$$

and the corresponding dual approximate solution becomes:

$$\begin{aligned}\bar{\theta}(\eta) &= 0.2369245422 \cdot e^{-0.5134938585\cdot\eta} + (1 + 1.0513455728 \cdot \eta)e^{-1.6176807383\cdot\eta} + \\ &+(0.0238401179 - 0.0020255651 \cdot \eta + 0.0000568573 \cdot \eta^2)e^{-0.1207882199\cdot\eta} + \\ &+(0.8098858748 + 0.2652845586 + 0.0285288295 \cdot \eta^2)e^{-2.4499501993\cdot\eta} + \\ &+(-1.0706505351 + 0.4609131356 \cdot \eta + 0.0444370182 \cdot \eta^2)e^{-1.2249750996\cdot\eta}\end{aligned} \tag{A2}$$

(a_3) the parameter $k = 0.25$, the Prandtl number $pr = 2.5$.

$$\begin{aligned}\bar{\theta}(\eta) &= -0.0000694691 \cdot e^{-0.0373028427\cdot\eta} + (1 - 0.6822337697 \cdot \eta)e^{-1.1414897224\cdot\eta} + \\ &+(-0.4228006041 - 0.1276408784 \cdot \eta - 0.7048478809 \cdot \eta^2)e^{-2.0265756010\cdot\eta} + \\ &+(-0.2530559522 - 0.5915096926 \cdot \eta - 0.3170935172 \cdot \eta^2)e^{-4.0531512020\cdot\eta} + \\ &+(0.6759260256 + 0.0914555047 \cdot \eta - 0.0099048402 \cdot \eta^2)e^{-0.9223887212\cdot\eta}\end{aligned} \tag{A3}$$

and the corresponding dual approximate solution becomes:

$$\begin{aligned}\bar{\theta}(\eta) &= 0.0001260254 \cdot e^{-0.0745075617\cdot\eta} + (1 - 0.0964643097 \cdot \eta)e^{-1.1786944415\cdot\eta} + \\ &+(-0.3203284037 + 1.8308083903 \cdot \eta - 0.0762347077 \cdot \eta^2)e^{-2.6623999026\cdot\eta} + \\ &+(-0.3417840921 - 0.4098840584 \cdot \eta - 0.0321843260 \cdot \eta^2)e^{-1.5582130229\cdot\eta} + \\ &+(0.6619864704 + 0.8089615723 \cdot \eta + 0.3222124279 \cdot \eta^2)e^{-5.3247998053\cdot\eta}\end{aligned} \tag{A4}$$

(a_4) the parameter $k = 0.15$, the Prandtl number $pr = 0.5$.

$$\begin{aligned}\bar{\theta}(\eta) &= 1.0983077175 \cdot e^{-0.4534958469\cdot\eta} + (1 + 0.4654950159 \cdot \eta)e^{-1.5576827266\cdot\eta} + \\ &+(-1.5363389724 + 0.3221215358 \cdot \eta - 0.0234501255 \cdot \eta^2)e^{-1.1308627520\cdot\eta} + \\ &+(0.0026808712 + 0.0000481427 \cdot \eta + 1.652544 \cdot 10^{-6} \cdot \eta^2)e^{-0.0266758723\cdot\eta} + \\ &+(0.4353503835 + 0.1426803574 \cdot \eta + 0.0157885694 \cdot \eta^2)e^{-2.2617255040\cdot\eta}\end{aligned} \tag{A5}$$

and the corresponding dual approximate solution becomes:

$$\begin{aligned}\bar{\theta}(\eta) &= 0.5391981597 \cdot e^{-0.4822945356\cdot\eta} + (1 + 0.5250981944 \cdot \eta)e^{-1.5864814153\cdot\eta} + \\ &+(0.3818837053 - 0.0092643162 \cdot \eta + 0.0000912270 \cdot \eta^2)e^{-0.1278543543\cdot\eta} + \\ &+(0.3480470015 + 0.1414195195 \cdot \eta + 0.0192266212 \cdot \eta^2)e^{-2.4640824681\cdot\eta} + \\ &+(-1.2691288666 + 0.2082420703 \cdot \eta + 0.0374340788 \cdot \eta^2)e^{-1.2320412340\cdot\eta}\end{aligned} \tag{A6}$$

The influence of the temperature distribution parameter k on the heat transfer is presented below. In this way, we provide the approximate analytical solutions for the case of $pr = 1.5$ and different values for k.

(a_5) In this case, we consider $k = 0.5$ and $pr = 0.5$.

$$\begin{aligned}\bar{\theta}(\eta) &= 0.0007206409 \cdot e^{-0.0000131202\cdot\eta} + (1 - 0.1316345278 \cdot \eta)e^{-1.1042000000\eta} + \\ &+(-1.0617752958 - 0.2671398226 \cdot \eta - 0.0590973088 \cdot \eta^2)e^{-1.5423591909\cdot\eta} + \\ &+(0.9992265151 - 0.0158696110 \cdot \eta + 0.0001546813 \cdot \eta^2)e^{-0.4381723112\cdot\eta} + \\ &+(0.0618281397 + 0.0411022791 \cdot \eta + 0.0096407838 \cdot \eta^2)e^{-3.0847183818\cdot\eta}\end{aligned} \tag{A7}$$

and the corresponding dual approximate solution is:

$$\begin{aligned}\bar{\theta}(\eta) &= 0.5513428358 \cdot e^{-0.1531064052\cdot\eta} + (1 + 2.1654964846 \cdot \eta)e^{-1.2572932849\cdot\eta} + \\ &+(-0.5837332313 + 0.1717462354 \cdot \eta - 0.3926304130 \cdot \eta^2)e^{-2.2051877057\cdot\eta} + \\ &+(0.4350443625 + 0.4520872315 \cdot \eta + 0.1673037370 \cdot \eta^2)e^{-4.4103754114\cdot\eta} + \\ &+(-0.4026539670 - 1.6609327359 \cdot \eta + 0.2537560261 \cdot \eta^2)e^{-1.1010008259\cdot\eta}\end{aligned} \tag{A8}$$

(a_6) In the second case, if $k = 0.15$ and $pr = 1$, then:

$$\begin{aligned}\bar{\theta}(\eta) = {} & 2.0683347602 \cdot e^{-0.9155012717 \cdot \eta} + (1 + 0.6833539452 \cdot \eta) e^{-2.0196881514 \cdot \eta} + \\ & + (-0.8031347222 - 0.7492677018 \cdot \eta - 0.1062182432 \cdot \eta^2) e^{-2.2813648143 \cdot \eta} + \\ & + (-1.2654357598 + 0.0862848192 \cdot \eta - 0.0427535328 \cdot \eta^2) e^{-1.1406824071 \cdot \eta} + \\ & + (0.0002357217 + 0.0000111023 \cdot \eta + 2.111508 \cdot 10^{-7} \cdot \eta^2) e^{-0.0364955274 \cdot \eta}\end{aligned} \tag{A9}$$

and the corresponding dual approximate solution is:

$$\begin{aligned}\bar{\theta}(\eta) = {} & 0.1878857950 \cdot e^{-0.4637756403 \cdot \eta} + (1 + 1.2766230888 \cdot \eta) e^{-1.5679625200 \cdot \eta} + \\ & + (0.0201352353 - 0.0009567685 \cdot \eta + 0.0000525361 \cdot \eta^2) e^{-0.0600476542 \cdot \eta} + \\ & + (1.1008756684 + 0.3253629902 \cdot \eta + 0.0338366627 \cdot \eta^2) e^{-2.3284690680 \cdot \eta} + \\ & + (-1.3088966989 + 0.5018533528 \cdot \eta + 0.0380250588 \cdot \eta^2) e^{-1.1642345340 \cdot \eta}\end{aligned} \tag{A10}$$

(a_7) In the third case, if $k = 0.15$ and $pr = 2.25$:

$$\begin{aligned}\bar{\theta}(\eta) = {} & 0.0752690301 \cdot e^{-1.3036641988 \cdot \eta} + (1 - 0.7216448042 \cdot \eta) e^{-2.4078510785 \cdot \eta} + \\ & + (-0.3478069740 - 0.4476541650 \cdot \eta - 0.2238753041 \cdot \eta^2) e^{-6.1184936238 \cdot \eta} + \\ & + (0.6232764356 + 0.4531574839 \cdot \eta - 0.1414849066 \cdot \eta^2) e^{-1.9550599322 \cdot \eta} + \\ & + (-0.3507384917 + 0.1210593773 \cdot \eta + 1.3248866865 \cdot \eta^2) e^{-3.0592468119 \cdot \eta}\end{aligned} \tag{A11}$$

and the corresponding dual approximate solution is:

$$\begin{aligned}\bar{\theta}(\eta) = {} & -0.0094833474 \cdot e^{-1.8199222326 \cdot \eta} + (1 + 4.8903828049 \cdot \eta) \cdot e^{-2.9241091123 \cdot \eta} + \\ & + (-0.2794803592 - 3.8038471274 \cdot \eta - 1.1301670707 \cdot \eta^2) e^{-3.4371389008 \cdot \eta} + \\ & + (0.2022965663 + 0.1763166133 \cdot \eta - 0.0935804838 \cdot \eta^2) e^{-1.7185694504 \cdot \eta} + \\ & + (0.0866671403 - 0.0267283075 \cdot \eta + 0.0022982197 \cdot \eta^2) e^{-0.6143825706 \cdot \eta}\end{aligned} \tag{A12}$$

In this way, we can construct other accurate approximate solutions.

References

1. Sparrow, E.M.; Cess, R.D. Temperature dependent heat sources or sinks in a stagnation point flow. *Appl. Sci. Res.* **1961**, *A10*, 185. [CrossRef]
2. Topper, L. Heat transfer in cylinders with heat generation. *Am. Inst. Chem. Fagug. J.* **1955**, *463*, 463–466. [CrossRef]
3. Khashi, N.S.; Waini, I.; Kasim, A.R.M.; Zainal, N.A.; Ishak, A.; Pop, I. Magnetohydrodynamic and viscous dissipation effects on radiative heat transfer of non-Newtonian fluid flow past a nonlinearly shrinking sheet: Reiner–Philippoff model. *Alex. Eng. J.* **2022**, *61*, 7605–7617. [CrossRef]
4. Vajravelu, K.; Hadjinicolaou, A. Heat transfer in a viscous fluid over a stretching sheet with viscous dissipation and internal heat generation. *Int. Comm. Heat Mass Transf.* **1993**, *20*, 417–430. [CrossRef]
5. Xu, H. Mixed convective flow of a hybrid nanofluid between two parallel inclined plates under wall-slip condition. *Appl. Math. Mech.-Engl. Ed.* **2022**, *43*, 113–126. [CrossRef]
6. Hayat, T.; Muhammad, K.; Alsaedi, A. Melting effect and Cattaneo-Christov heat flux in fourth-grade material flow through a Darcy-Forchheimer porous medium. *Appl. Math. Mech.-Engl. Ed.* **2021**, *42*, 1787–1798. [CrossRef]
7. Bararnia, H.; Gorji, M.; Domairry, G. An Analytical Study of Boundary Layer Flows on a Continuous Stretching Surface. *Acta Appl. Math.* **2009**, *106*, 125–133. [CrossRef]
8. Khan, N.S.; Islam, S.; Gul, T.; Khan, I.; Khan, W.; Ali, L. Thin film flow of a second grade fluid in a porous medium past a stretching sheet with heat transfer. *Alex. Eng. J.* **2018**, *57*, 1019–1031. [CrossRef]
9. Khan, N.S.; Gul, T.; Islam, S.; Khan, I.; Alqahtani, A.M.; Alshomrani, A.S. Magnetohydrodynamic Nanoliquid Thin Film Sprayed on a Stretching Cylinder with Heat Transfer. *Appl. Sci.* **2017**, *7*, 271. [CrossRef]
10. Khan, N.S.; Gul, T.; Kumam, P.; Shah, Z.; Islam, S.; Khan, W.; Zuhra, S.; Arif, S. Influence of Inclined Magnetic Field on Carreau Nanoliquid Thin Film Flow and Heat Transfer with Graphene Nanoparticles. *Energies* **2019**, *12*, 1459. [CrossRef]
11. Khan, N.S.; Zuhra, S. Boundary layer flow and heat transfer in a thin-film second-grade nanoliquid embedded with graphene nanoparticles. *Adv. Mech. Eng.* **2019**, *11*, 1–11. [CrossRef]
12. Zuhra, S.; Khan, N.S.; Khan, M.A.; Islam, S.; Khan, W.; Bonyah, E. Flow and heat transfer in water based liquid film fluids dispensed with graphene nanoparticles. *Results Phys.* **2018**, *8*, 1143–1157. [CrossRef]
13. Bilal, A.M.; Alsaedi, A.; Hayat, T.; Shehzad, S.A. Convective Heat and Mass Transfer in Three-Dimensional Mixed Convection Flow of Viscoelastic Fluid in Presence of Chemical Reaction and Heat Source/Sink. *Comp. Math. Math. Phys.* **2017**, *57*, 1066–1079. [CrossRef]

14. Shehzad, S.A.; Hayat, T.; Alsaedi, A. Flow of a thixotropic fluid over an exponentially stretching sheet with heat transfer. *J. Appl. Mech. Tech. Phy.* **2016**, *57*, 672–680. [CrossRef]
15. Alizadeh, Y.; Mosaddeghi, M.R.; Khazayinejad, M. Semi-analytical assessment of heat transfer rate for MHD transient flow in a semi-porous channel considering heat source and slip effect. *Waves Random Complex Media* **2021**, 1–23. [CrossRef]
16. Yan, H.; Sedighi, M.; Xie, H. Thermally induced diffusion of chemicals under steady-state heat transfer in saturated porous media. *Int. J. Heat Mass Tran.* **2020**, *153*, 119664. [CrossRef]
17. Nadeem, J.; Marwat, D.N.K.; Khan, T.S. Heat transfer in viscous flow over a heated cylinder of nonuniform radius. *Ain Shams Eng. J.* **2021**, *12*, 4189–4199.
18. Abbasi, A.; Khan, S.U.; Farooq, W.; Mughal, F.M.; Khan, M.I.; Prasannakumara, B.C.; El-Wakad, M.T.; Guedri, K.; Galal, A.M. Peristaltic flow of chemically reactive Ellis fluid through an asymmetric channel: Heat and mass transfer analysis. *Ain Shams Eng. J.* **2023**, *14*, 101832. [CrossRef]
19. Xie, W.A.; Xi, G.N. Flow instability and heat transfer enhancement of unsteady convection in a step channel. *Alex. Eng. J.* **2022**, *61*, 7377–7391. [CrossRef]
20. Abdelaziz, A.H.; El-Maghlany, W.M.; El-Din, A.A.; Alnakeeb, M.A. Mixed convection heat transfer utilizing Nanofluids, ionic Nanofluids, and hybrid nanofluids in a horizontal tube. *Alex. Eng. J.* **2022**, *61*, 9495–9508. [CrossRef]
21. Muhammad, K.; Hayat, T.; Alsaedi, A. OHAM analysis of fourth-grade nanomaterial in the presence of stagnation point and convective heat-mass conditions. *Waves Random Complex Media* **2021**, 1–17. [CrossRef]
22. Mabood, F.; Lorenzini, G.; Pochai, N.; Ibrahim, S.M. Effects of prescribed heat flux and transpiration on MHD axisymmetric flow impinging on stretching cylinder. *Contin. Mech. Therm.* **2016**, *28*, 1925–1932. [CrossRef]
23. Eid, M.R.; Nafe, M.A. Thermal conductivity variation and heat generation effects on magneto-hybrid nanofluid flow in a porous medium with slip condition. *Waves Random Complex Media* **2020**. [CrossRef]
24. Boumaiza, N.; Kezzar, M.; Eid, M.R.; Tabet, I. On numerical and analytical solutions for mixed convection Falkner-Skan flow of nanofluids with variable thermal conductivity. *Waves Random Complex Media* **2019**. [CrossRef]
25. Gireesha, B.J.; Keerthi, M.L.; Sowmya, G. Effects of stretching/shrinking on the thermal performance of a fully wetted convective-radiative longitudinal fin of exponential profile. *Appl. Math. Mech.-Engl. Ed.* **2022**, *43*, 389–402. [CrossRef]
26. Waini, I.; Ishak, A.; Pop, I. Magnetohydrodynamic flow past a shrinking vertical sheet in a dusty hybrid nanofluid with thermal radiation. *Appl. Math. Mech.-Engl. Ed.* **2022**, *43*, 127–140. [CrossRef]
27. Tang, Q.; Huang, Y. Parallel finite element computation of incompressible magnetohydrodynamics based on three iterations. *Appl. Math. Mech.-Engl. Ed.* **2022**, *43*, 141–154. [CrossRef]
28. Cveticanin, L. Exact Closed-Form Solution for the Oscillator with a New Type of Mixed Nonlinear Restitution Force. *Mathematics* **2023**, *11*, 596. [CrossRef]
29. Raduca, M.; Hatiegan, C.; Pop, N.; Raduca, E.; Gillich, G.-R. Finite element analysis of heat transfer in transformers from high voltage stations. *J. Therm. Anal. Calorim.* **2014**, *18*, 1355–1360. [CrossRef]
30. Martin, M.J.; Boyd, I.D. Momentum and heat transfer in a laminar boundary layer with slip flow. *J. Thermo Heat Trans.* **2006**, *20*, 710–719. [CrossRef]
31. Anderson, H.I. Slip flow past a stretching surface. *Acta Mech.* **2002**, *158*, 121–125. [CrossRef]
32. Khan, N.S.; Zuhra, S.; Shah, Z.; Bonyah, E.; Khan, W.; Islam, S.; Khan, A. Hall current and thermophoresis effects on magnetohydrodynamic mixed convective heat and mass transfer thin film flow. *J. Phys. Commun.* **2019**, *3*, 035009. [CrossRef]
33. Nayak, M.K.; Mabood, F.; Dogonchi, A.S.; Ramadan, K.M.; Tlili, I.; Khan, W.A. Entropy optimized assisting and opposing non-linear radiative flow of hybrid nanofluid. *Waves Random Complex Media* **2022**, 1–22. [CrossRef]
34. Cortell, R. Viscous flow and heat transfer over a nonlinearly stretching sheet. *Appl. Math. Comput.* **2007**, *184*, 864–873. [CrossRef]
35. Alam, A.; Marwat, D.N.K. Heat and mass transfer on a stretching/shrinking and porous sheet of variable thickness with suction and injection. *Proc. Inst. Mechanical Eng. Part C J. Mech. Eng.* **2021**, *235*, 5297–5308. [CrossRef]
36. Marinca, V.; Herisanu, N. *The Optimal Homotopy Asymptotic Method-Engineering Applications*; Springer: Berlin/Heidelberg, Germany, 2015.
37. Marinca, V.; Ene, R.D.; Marinca, B.; Negrea, R. Different approximations to the solution of upper-convected Maxwell fluid over a porous stretching plate. *Abstr. Appl. Anal.* **2014**, *2014*, 139314. [CrossRef]
38. Ene, R.D.; Marinca, V. Approximate solutions for steady boundary layer MHD viscous flow and radiative heat transfer over an exponentially porous stretching sheet. *Appl. Math. Comput.* **2015**, *269*, 389–401. [CrossRef]
39. Ene, R.D.; Szabo, M.A.; Danoiu, S. Viscous flow and heat transfer over a permeable shrinking sheet with partial slip. *Mater Plast.* **2015**, *52*, 408–412.
40. Marinca, V.; Ene, R.D. Dual approximate solutions of the unsteady viscous flow over a shrinking cylinder with Optimal Homotopy Asymptotic Method. *Adv. Math. Phys.* **2014**, 417643. [CrossRef]
41. Ene, R.D.; Pop, N. Dual approximate solutions for the chemically reactive solute transfer in a viscous fluid flow. *Waves Random Complex Media* **2021**, 1–23. [CrossRef]
42. Ullah, H.; Nawaz, R.; Islam, S.; Idrees, M.; Fiza, M. The optimal homotopy asymptotic method with application to modified Kawahara equation. *J. Assoc. Arab. Univ. Basic Appl. Sci.* **2015**, *18*, 82–88. [CrossRef]
43. Almousa, M.; Ismail, A. Optimal Homotopy Asymptotic Method for Solving the Linear Fredholm Integral Equations of the First Kind. *Abstr. Appl. Anal.* **2013**, *2013*, 278097. [CrossRef]

44. Golbabai, A.; Fardi, M.; Sayevandc, K. Application of the optimal homotopy asymptotic method for solving a strongly nonlinear oscillatory system. *Math. Comput. Model.* **2013**, *58*, 1837–1843. [CrossRef]
45. Alomari, A.K.; Anakira, N.R.; Hashim, I. Multiple Solutions of Problems in Fluid Mechanics by Predictor Optimal Homotopy Asymptotic Method. *Adv. Mech. Eng.* **2014**, *6*, 372537. [CrossRef]
46. Marinca, V.; Herisanu, N. Application of Optimal Homotopy Asymptotic Method for solving nonlinear equations arising in heat transfer. *Int. Commun. Heat Mass.* **2008**, *35*, 710–715 [CrossRef]
47. Ullah, H.; Islam, S.; Idrees, M.; Arif, M. Solution of Boundary Layer Problems with Heat Transfer by Optimal Homotopy Asymptotic Method. *Abstr. Appl. Anal.* **2013**, *2013*, 324869. [CrossRef]
48. Waqar, K. Optimal homotopy asymptotic method for heat transfer in hollow sphere with robin boundary conditions. *Heat Transf. Asian Res.* **2014**, *43*, 124–133.
49. Ene, R.D.; Marinca, V.; Negrea, R. Optimal Homotopy Asymptotic Method for viscous boundary layer flow in unbounded domain. In Proceedings of the 16th International Symposium on Symbolic and Nnumeric Algoritms for Scientific Computing (SYNASC 2014), Timisoara, Romania, 22–25 September 2014.
50. Ene, R.D.; Petrisor, C. Some mathematical approaches on the viscous flow problem on a continuous stretching surface: Nonlinear stability and dual approximate analytic solutions. *AIP Conf. Proc.* **2020**, *2293*, 350004.
51. Daftardar-Gejji, V.; Jafari, H. An iterative method for solving nonlinear functional equations. *J. Math. Anal. Appl.* **2006**, *316*, 753–763. [CrossRef]
52. Giles, R.V. *Theory and Problems of the Hydraulics*, 2nd ed.; Schaum's Outline Series; McGraw Hill Book Company: New York, NY, USA, 1977.
53. Greenshields, C.; Weller, H.G. *Notes on Computational Fluid Dynamics:General Principles*; CFD Direct Limited: Reading, UK, 2022.